THE JOURNAL OF PHYSICAL CHEMISTRY C

Article

pubs.acs.org/JPCC

# Improvement of Hematite as Photocatalyst by Doping with Tantalum

Xinsheng Zhang,[†,‡,§] Huicheng Li,[‡] Shijun Wang,[†] Fu-Ren F. Fan,[†] and Allen J. Bard*[,†]

[†]Center for Electrochemistry, Department of Chemistry and Biochemistry, The University of Texas at Austin, University Station A5300, Austin, Texas 78712, United States

[‡]State-Key Laboratory of Chemical Engineering, East China University of Science and Technology, Meilong Road 130, Shanghai 200237, China

**ABSTRACT:** The use of tantalum as a highly effective dopant for hematite photoelectrochemistry (PEC) has shown contradictory results in previous reports. We show here through screening of different compositions by scanning electrochemical microscopy that Ta doping significantly improves the PEC performance of dropcast films on fluorine-doped tin oxide (FTO). In studies with larger electrodes, a 2% Ta-doped hematite photoanode fabricated at 500 °C shows the highest improvement of photoactivity, which is ~32 times higher than pure hematite even under visible light. At fabrication temperature higher than 500 °C (e.g., 600, 680 °C), the substrate FTO becomes more resistive and the dopant Ta prefers to segregate from the bulk phase ($\alpha$-$Fe_2O_3$) and forms tantalum fluoride oxide ($TaO_2F$), which may act as charge-carrier recombination centers, and the corresponding Ta-doped samples show much lower photoactivities. Ta-doped hematite samples show stronger (110) diffraction as compared with the pure $\alpha$-$Fe_2O_3$. We show that the doping of Ta induced a preferential growth along the {001} basal plane, which has been reported to have good conductivity. We found the conductivity of the Ta-doped hematite was improved up to at least about one order of magnitude after the incorporation of Ta, with the improved carrier mobility decreasing recombination of the photogenerated holes and electrons.

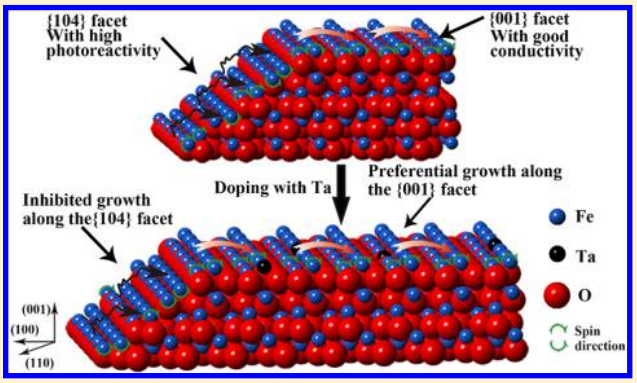


## 1. INTRODUCTION

Hardee and Bard[1] first investigated hematite ($\alpha$-$Fe_2O_3$) as a material for photoelectrochemistry in 1976, reporting that $\alpha$-$Fe_2O_3$ showed response to light of wavelength ≤500 nm. Since that time $\alpha$-$Fe_2O_3$ has been extensively investigated as a promising photocatalysts material for water splitting because of its appropriate bandgap (~2.2 eV), good PEC stability, and low cost. Despite these advantages, the photoactivity of $\alpha$-$Fe_2O_3$ suffers from limitations that result in low efficiency. These include relatively low absorptivity in the visible region, short carrier lifetime (~10−12 $\mu$s), and short hole diffusion length (2−4 nm). These can be tied to its low carrier mobility.

Extensive previous studies on many oxide semiconductors showed that doping is an effective method to ameliorate these shortcomings, and elements such as Si,[2−4] Ti,[4−7] Al,[8] Nb,[9] Sn,[6,10,11] Cr,[12] Mo,[12] Ni,[13] Mg,[14,15] and Zn[5,16] have been incorporated into $\alpha$-$Fe_2O_3$ as dopants to enhance the photoactivity of hematite. However, because the number of different dopants that can be tested and their concentrations are very high, rapid testing methods are needed to screen potential dopant candidates.

Our group has developed a rapid and effective method based on scanning electrochemical microscopy (SECM)[17] for preparing arrays and screening different concentrations of dopants, and even multiple dopants, to optimize dopant concentrations.[18] The method has recently been applied to dope $\alpha$-$Fe_2O_3$-based photocatalyst, and an array of effective dopants has been reported.[19,20] We have screened tantalum as a highly effective dopant for $\alpha$-$Fe_2O_3$ by the modified SECM method, and found that the Ta-doped $\alpha$-$Fe_2O_3$ showed significantly enhanced photoactivity for PEC reactions in both the UV−visible and visible light regions compared with pure $\alpha$-$Fe_2O_3$. Tantalum has been investigated previously as a dopant for $\alpha$-$Fe_2O_3$ by Aroutiounian et al.[21] and by Sartoretti et al.[5] The results of these researches differed from each other. Aroutiounian et al.[21] reported that Ta-doped $\alpha$-$Fe_2O_3$ prepared by mixing $\alpha$-$Fe_2O_3$ with $Ta_2O_5$ and sintering at a high temperature (≥1000 °C) for a long time (≥30 h) showed improved behavior. In Sartoretti's work,[5] the addition of Ta in $\alpha$-$Fe_2O_3$, prepared by spray pyrolysis, showed no real obvious effect on the photoactivity of $\alpha$-$Fe_2O_3$, Our sample fabrication method is relatively facile and requires a much lower temperature (~500 °C) and shorter heating times (≤12 h).

**Special Issue:** Michael Grätzel Festschrift

**Received:** January 13, 2014
**Revised:** March 21, 2014

   dx.doi.org/10.1021/jp500395a | J. Phys. Chem. C XXXX, XXX, XXX−XXX

## 2. EXPERIMENTAL SECTION

**2.1. Chemicals.** FTO-coated glass (Pilkington, Toledo, OH) was used as a substrate and cut into 15 × 20 mm squares, followed by successive ultrasonic cleaning in ethanol and rinsing with deionized water. Fe $(NO_3)_3 \cdot 9H_2O$ (99.6%, J.T. Baker), $TaCl_5$ (99.99%, Aldrich), $TaF_5$ (99.99%, Aldrich), $Ta_2O_5$ (99.99%, <5 μm, Aldrich), $Na_2SO_4$ (anhydrous, 99.3%, Fisher), $Na_2SO_3$ (anhydrous, 99.4%, Fisher), methanol (biotech grade, 99.93%, Sigma-Aldrich), ethanol (absolute anhydrous, 99.98%, Pharmco-Aaper), ethylene glycol (99.9%, Fisher), glycerol (99.8%, Fisher), ether (anhydrous, 99.7%, Sigma-Aldrich), acetone (99.8%, Fisher), and 2-propanol (99.9%, Fisher) were used as received, and Milli-Q water was used to prepare all solutions. Tantalum chloride solutions were made with ethanol or methanol with a tantalum concentration of 0.05 M; then, they were diluted to 0.002 M with ethylene glycol. Other solutions of metal precursor were made with ethylene glycol containing 0.1 M metal salt.

**2.2. Preparation of Photocatalyst Arrays.** The photocatalyst arrays were prepared by a previously reported dispenser system (CH Instruments model 1550, Austin, TX)[17] consisting of a high-resolution 3-D positioner, a piezoelectric jetting (MicroJet AB-01-60, MicroFab, Plano, TX), and a sample platform controlled by a PC computer. The FTO (fluorine-doped tin oxide) substrate was placed on the platform, and the 3-D positioner moved the piezoelectric jetting in a preprogrammed pattern, while programmed voltage pulses were applied to the dispenser to eject the requested number of drops (~100 pL each) of the metal precursor solution onto the substrate. The first component (metal precursor solution) was loaded and dispensed in a preprogrammed pattern onto the FTO substrate. After flushing and washing the piezodispenser, the second component was loaded into the dispenser and dispensed into the existing pattern. The arrays were ramped from room temperature to 500 °C at a ramp rate of 2 °C/min and annealed at 500 °C for the desired time, for example, 3 h.

**2.3. Screening the Array.** A 400 μm diameter optical fiber (FT-400-URT, 3M, St. Paul, MN), coupled to a Xe lamp via a model 9091 five-axis fiber aligner (New Focus, San Jose, CA), was attached to the tip holder of a CHI model 900B SECM. The array was placed in a Teflon SECM cell with the FTO/photocatalyst working electrode exposed at the bottom through an O-ring. A Pt wire counter electrode and an Ag/AgCl reference electrode were used to complete the three-electrode electrochemical cell configuration. A solution of 0.1 M $Na_2SO_4$ and 0.1 M $Na_2SO_3$ as a sacrificial electron donor was used as the electrolyte in screening. A detailed schematic diagram of the SECM setup can be found in a previous report.[17] The optical fiber was positioned perpendicular to the working electrode surface and scanned laterally across the surface at a faster rate of 500 μm/s. The optical fiber tip was held and scanned 150 μm above the working electrode surface, while a given potential was applied to the working electrode array by the SECM potentiostat. The photocurrent produced during the scan was measured and recorded to produce a color-coded 2-D image.

**2.4. Characterization.** Glancing incidence angle X-ray diffraction (GIXRD) was performed with a Bruker-Norius D8 advanced diffractometer using a Cu Kα radiation source operated at 40 kV and 40 mA with an incidence angle of 1.0°. Samples for XRD were prepared on a glass slide using a 0.1 M Fe salt solutions containing different Ta salt contents. The solutions were coated on cleaned glass slides, followed by drying at 140 °C for 10 min in air after each coating with 50 μL of solution, and this process was repeated four times. X-ray photoelectron spectroscopy (XPS) was performed with a Kratos Axis Ultra DLD instrument (Manchester, U.K.) with a monochromatic Al X-ray source. Samples for XPS were prepared on cleaned FTO using a 0.01 M Fe salt solution containing different Ta salt contents.

**2.5. Photoelectrochemical Experiments.** To confirm the SECM screening results, we fabricated bulk films on FTO substrate with a larger area (1.5 cm × 2 cm) by a facile method. The tantalum salt solution with a tantalum concentration of 0.04 M was prepared with anhydrous methanol, which was diluted with $Fe(NO_3)_3$-ethylene glycol solution (0.04 M) to reach the planned concentration. 100 μL of prepared $Fe(NO_3)_3$ + Ta solution was dropped onto FTO substrate, followed by drying at 140 °C for 10 min in air. Then, the films were ramped from room temperature to 500 °C at a rate of 2 °C/min and annealed at 500 °C for 3 h. The PEC properties of each sample were obtained by using a three-electrode borosilicate glass cell equipped with a Pt-gauze counter electrode and a Ag/AgCl reference electrode. A potentiostat (CH Instruments, model 630D, Austin, TX) was used to perform electrochemical measurements. All PEC measurements were performed at room temperature. The prepared films were used as working electrodes and were clamped onto the glass cell via an O-ring with a 0.2 $cm^2$ geometric area exposed to the electrolyte solution and to light irradiation. The PEC experiments were carried out in either a solution of 0.1 M $Na_2SO_4$ and 0.1 M $Na_2SO_3$ or in 0.1 M $Na_2SO_4$ solution alone (i.e., with no sacrificial donor). Irradiation was achieved through the electrolyte solution by a Xe lamp (XBO 150 W, Osram, Munich, Germany) with an incident UV−visible light intensity of ~110 mW/$cm^2$. A UV cutoff filter ($\lambda$ > 420 nm) was used for visible-light irradiation, and the resulting visible-light intensity was ca. 100 mW/$cm^2$. A monochromator (Photon Technology International, Birmingham, NJ) was used in combination with a power meter (Newport Model 1830-C, Irvine, CA) and a silicon detector (Newport Model 818-UV) to measure incident photon to current conversion efficiencies (IPCEs). Electrochemical impedance spectroscopy (EIS) was performed using an Autolab instrument (PGSTAT30/FRA2) to obtain the Mott−Schottky plots at frequencies of 200, 500, and 1000 Hz and a peak-to-peak amplitude of 5 mV at each potential. Samples were prepared on cleaned FTO using 100 μL of 0.01 M Fe salt solutions with different Ta salt contents.

## 3. RESULTS AND DISCUSSION

**3.1. Screening Arrays by SECM.** As shown in Figure 1, the photocatalyst spots from left to right were 0, 0.5, 1.5, 2.0,

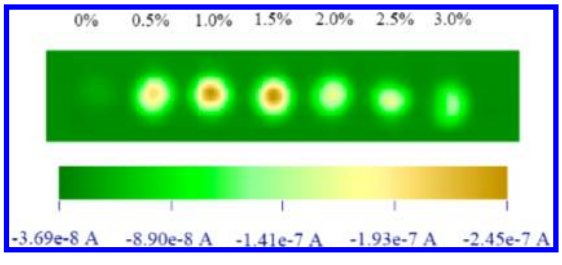


**Figure 1.** SECM image of Fe-Ta-O photocatalyst array at 0.2 V versus Ag/AgCl in 0.1 M $Na_2SO_4$ + 0.1 M $Na_2SO_3$ solution under UV−visible light.


dx.doi.org/10.1021/jp500395a | J. Phys. Chem. C XXXX, XXX, XXX−XXX

2.5, and 3.0% of tantalum relative to Fe (mole ratio), respectively. Twenty drops of 0.1 M iron salt were dispensed on each spot on FTO first, and then different drops of 0.002 M tantalum chloride solution were dropped in turn to control the dopant concentration of each spot as programmed. The relative number of drops determined the spot composition. The spot located at left corner had 20 drops of $Fe(NO_3)_3$ and was used as an internal standard. The applied potential was 0.2 V versus Ag/AgCl, and the electrolyte solution was a mixed solution of 0.1 M $Na_2SO_4$ and 0.1 M $Na_2SO_3$. The result indicates that incorporating a certain content of Ta in $\alpha$-$Fe_2O_3$ increased the anodic photocurrent with a maximum at ~1.0 to 1.5% Ta. The maximum was about four times that of a pure $\alpha$-$Fe_2O_3$ spot (63 nA). The photocurrent decreased with further increase, in agreement with Aroutiounian,[21] showing quite a large improvement in the photocurrent of Ta-doped $\alpha$-$Fe_2O_3$. There are a number of cases where the observed photoactivity depends on the material preparation method, for example, the difference of the photoactivity of Cr-doped $TiO_2$ prepared by a chemical-doping method and by ion implantation.[22] Different doping methods can lead to different defects and different electronic structures, but details of the physicochemical processes remain to be studied.

**3.2. Photocatalytic Activity.** The PEC performance of bulk iron oxide films doped with tantalum was studied using linear sweep voltammetry (LSV). Figure 2 shows the LSVs of

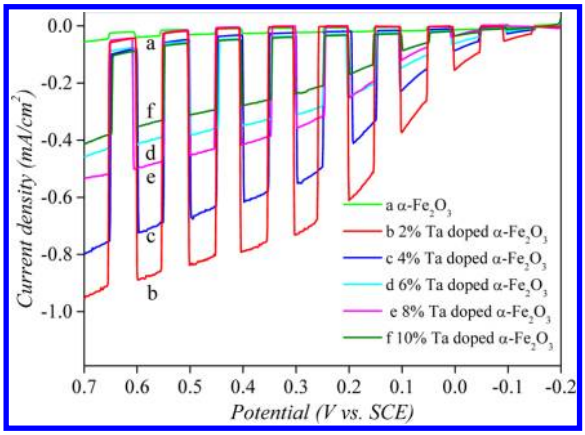


**Figure 2.** Chopped LSVs for $\alpha$-$Fe_2O_3$ with different Ta doping concentration under UV–visible irradiation. The sweep rate: 20 mV/s, electrolyte condition: 0.1 M $Na_2SO_3$ + 0.1 M $Na_2SO_4$.

bulk $\alpha$-$Fe_2O_3$ films containing different content of Ta in 0.1 M $Na_2SO_3$ + 0.1 M $Na_2SO_4$ aqueous solution under chopped UV–visible (a) and visible ($\lambda$ > 420 nm) (b) light irradiation.

Bulk $\alpha$-$Fe_2O_3$ films doped with Ta exhibited a significant increase in photocurrent relative to pure $\alpha$-$Fe_2O_3$ under both UV–visible and visible light irradiation relative to that of pure $\alpha$-$Fe_2O_3$. The photocurrent at 0.65 V versus Ag/AgCl of $\alpha$-$Fe_2O_3$ containing 2% Ta was ca. 33 times higher under UV–visible light irradiation and 32 times higher under visible light irradiation relative to that of pure $\alpha$-$Fe_2O_3$. The enhancements were even higher in the region of less positive potentials. An excess of Ta, however, is harmful to its photoactivity. The photocurrents of these films decreased with Ta content over 2%. These results with bulk films were in general accordance with those observed by SECM screening.

We had also compared the photocurrents between $\alpha$-$Fe_2O_3$ containing 2% Ta and pure $\alpha$-$Fe_2O_3$ in a 0.1 M $Na_2SO_4$ aqueous solution, where the anodic photocurrent is attributed to water oxidation (Figure 3). The photocurrent of a sample

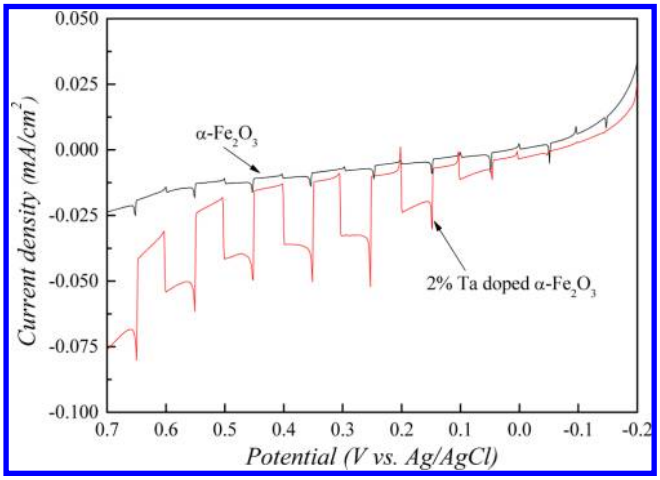


**Figure 3.** Chopped LSVs for pure $\alpha$-$Fe_2O_3$ and 2% Ta-doped $\alpha$-$Fe_2O_3$ under UV–visible irradiation. The sweep rate: 20 mV/s, electrolyte condition: 0.1 M $Na_2SO_4$.

with 2% Ta was seven times higher than that of pure iron oxide. Their photocurrents in 0.1 M $Na_2SO_4$ aqueous solution were far less than those in mixed solution of 0.1 M $Na_2SO_3$ and 0.1 M $Na_2SO_4$ aqueous solution. (See Figure 4 and the description

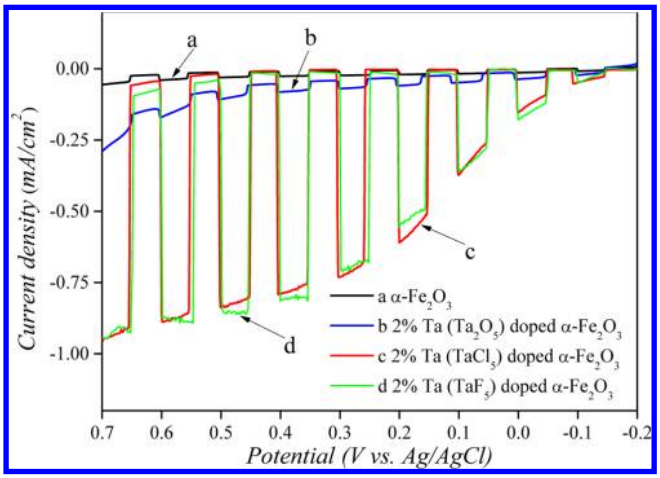


**Figure 4.** Chopped LSVs for pure $\alpha$-$Fe_2O_3$ and $\alpha$-$Fe_2O_3$ doped with different Ta precursor under UV–visible irradiation. The sweep rate: 20 mV/s, electrolyte condition: 0.1 M $Na_2SO_3$ + 0.1 M $Na_2SO_4$.

shown later.) The smaller values for water oxidation, about 3 and 5% of the values in mixed solutions for iron oxide with 2% Ta and pure iron oxide, respectively, are related to the more difficult water oxidation step and suggest better results with an oxygen evolution reaction (OER) catalyst.

To explore the role of tantalum in doped $\alpha$-$Fe_2O_3$ films, tantalum chloride, tantalum fluoride, and tantalum oxide crystals were used as raw materials to make films. The results in Figure 4 show that the photocurrent of films doped with tantalum chloride is much higher than those doped with tantalum oxide. The current density of the $\alpha$-$Fe_2O_3$ photoanode doped with $TaF_5$ is almost the same as that with $TaCl_5$, indicating that the anion (i.e., Cl, F) of tantalum salt has no obvious effect on the photoactivity of an $\alpha$-$Fe_2O_3$ photoanode.


dx.doi.org/10.1021/jp500395a | J. Phys. Chem. C XXXX, XXX, XXX–XXX

The photocurrent of films doped with tantalum oxide is only 8% of the photocurrent of films by tantalum chloride, but it is still about three times higher than that of an undoped iron oxide. In the precursor solution, tantalum chloride could be homogenously dissolved, while tantalum oxide particles are just suspended in the solution, thus tantalum ion in tantalum chloride could diffuse more easily and mix more sufficiently with iron ion than particulate tantalum oxide dopant. On one hand, the use of tantalum chloride may lead to more uniform tantalum ion distribution in the vicinity of formed tantalum-chloride-doped $\alpha$-$Fe_2O_3$ film as compared with a tantalum-oxide-doped sample. On the other hand, Ta in tantalum-oxide-doped samples might prefer to exist as its original $Ta_2O_5$ phase rather than substituting for $Fe^{3+}$ in the hematite lattice.

The photocurrent activities of $\alpha$-$Fe_2O_3$ films fabricated at different temperatures (400, 500, 600, and 680 °C) are shown in Figure 5. The photocatalytic activity of the sample varies with preparation temperature and $\alpha$-$Fe_2O_3$ film prepared at 500 °C shows the highest photocatalytic activity than other samples. However, the FTO is not stable at temperatures above about 550°, so the large decreases probably represent loss of conductivity in the FTO. In Sartoretti's work,[5] it was reported that thermal annealing could decrease the disorder, caused by $Fe_3O_4$ or FeO and unfavorable for the photocatalytic property, and could improve the ordering of crystal structure and thus enhance the photocatalytic performance of $\alpha$-$Fe_2O_3$. We also employed the XRD characterization shown later to study samples prepared at higher temperatures compared with those prepared at 500 °C.

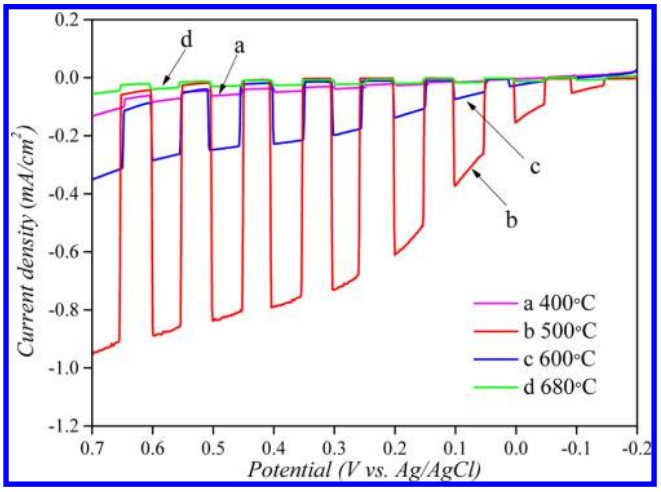


**Figure 5.** Chopped LSVs for 2% Ta-doped $\alpha$-$Fe_2O_3$ prepared at different temperatures under UV−visible irradiation. The sweep rate: 20 mV/s, electrolyte condition: 0.1 M $Na_2SO_3$ + 0.1 M $Na_2SO_4$.

**3.3. X-Ray Diffraction (XRD).** X-ray diffraction spectra of pure $\alpha$-$Fe_2O_3$ and Ta-doped $\alpha$-$Fe_2O_3$ prepared at 500 °C are shown in Figure 6 a. $\alpha$-$Fe_2O_3$ (JCPDS 79-1741) is identified as the major phase in all samples studied, and no other impurity phases can be found. Because $Ta^{5+}$ has a similar radius as $Fe^{3+}$ in high-spin state, which are 0.64 and 0.635 Å,[23] respectively, even if the $Ta^{5+}$ is incorporated at a $Fe^{3+}$ site in the hematite lattice no observable shift can be found in the XRD spectra. However, the obvious change of the relative intensity of (104) and (110) peaks with increasing tantalum content (Figure 6a) is significant. To evaluate the degree of orientation, the Lotgering method[24] was adopted

$$f = \frac{P - P_0}{1 - P_0} \tag{1}$$

where

$$P = \frac{I(110)}{\sum I(hkl)} \tag{2}$$

$$P_0 = \frac{I_o(110)}{\sum I_0(hkl)} \tag{3}$$

$\Sigma I(hkl)$ is the sum of the XRD peak intensities for the Ta-doped hematite and $\Sigma I_0(hkl)$ is the sum of the peak intensities for the pure one. As shown in Figure 8, the (110) orientation

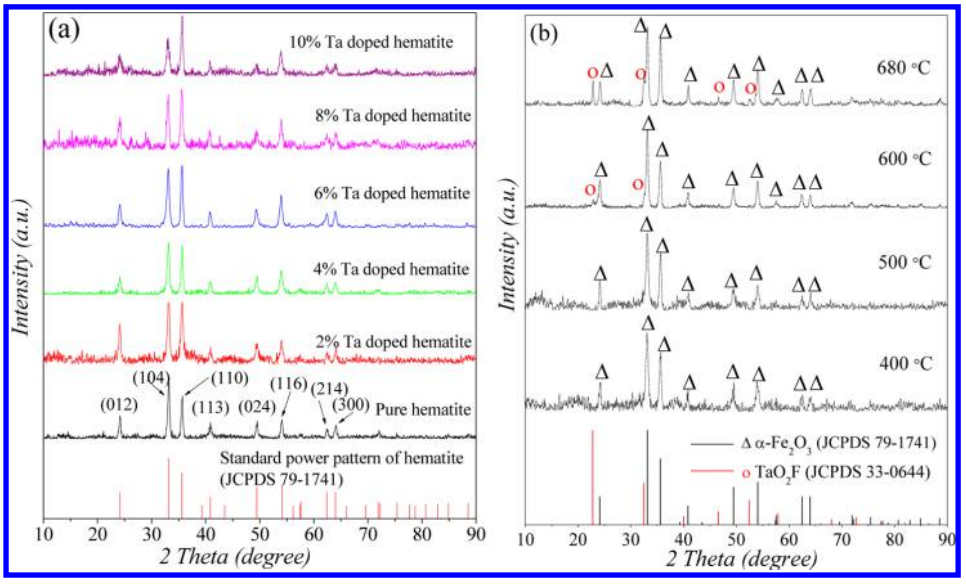


**Figure 6.** XRD spectra for (a) $\alpha$-$Fe_2O_3$ doped with different Ta doping concentration and (b) 2% Ta-doped $\alpha$-$Fe_2O_3$ prepared at different temperatures.


dx.doi.org/10.1021/jp500395a | J. Phys. Chem. C XXXX, XXX, XXX−XXX

and the inhibition represented by the peak (012) and (104) can be observed after the doping of Ta.

Our thin film samples were fabricated on a glass substrate, and the thickness of the film was about several hundred nanometers. To avoid intense signal from the substrate and obtain a stronger signal from the thin film sample, GIXRD analysis was performed. In previous studies, it was indicated that the intensity of the peaks in the XRD patterns recorded with the conventional $2\theta/\theta$ mode showed the same changes in trends with the results from the GIXRD. The crystallographic orientation of ZnO thin films indicated by GIXRD also correlated well with the conventional XRD patterns reported by Lavčević et al.[25] In Chiu et al.[26] and Merschjann et al.,[27] the Lotgering factor was also adopted to describe the preferred orientation shown in the GIXRD patterns. Even with our less rigorous use of the Lotgering method, the conclusions regarding the preferential growth induced by doping with Ta are probably acceptable.

A similar XRD pattern has also been observed in the Si-doped hematite reported by Grätzel et al.[3] Stronger (110) diffraction means hematite prefers to grow along the {001} basal plane. From the point of the crystal face stability, we ascribe this to the high bonding energies of Ta-O and Si-O, which are 805 and 798 kJ·mol$^{-1}$, respectively, and are about twice that of Fe-O (409 kJ·mol$^{-1}$),[28] and thus the substitution of Ta for Fe in the hematite lattice might lower the surface energy of {001} facets, which is ~2.31 kJmol$^{-1}$ and is higher than that of {102} and {100} facets under normal conditions,[29] and make the {001} crystal planes more stable. Consequently, the presence of Ta or Si dopants might exert a positive influence on the growth rate of {001} facets in the growth of the hematite polycrystalline film, resulting in a preferential orientation along the {001} basal planes (as described in Figure 7). A similar example can be seen in research by Yang et al. [30]

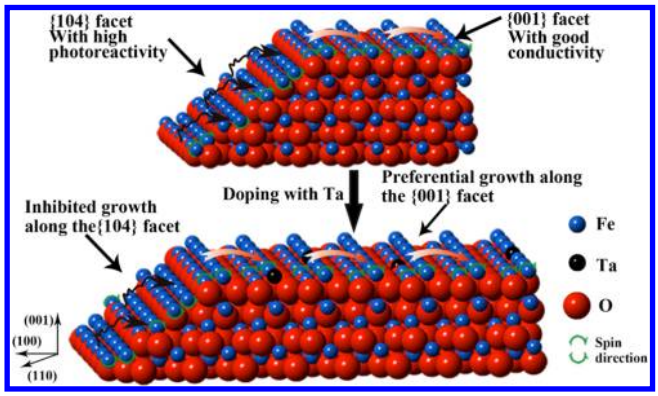


**Figure 7.** Model of pure (top) and Ta-doped hematite (bottom) with the {001} and {104} surfaces.

about the synthesis of $TiO_2$ single crystals with a large percentage of reactive facets, in which the introduced fluorine has a strong bonding to Ti and improves the stability of {001} facets, which are reported to be especially reactive but not thermodynamically stable under normal conditions.

The conductivity along the {001} crystal facets is reported to be up to four orders of magnitude larger than that of the [110] direction.[31] This agrees well with conductivity measurements as described later. Viewed from the [110] direction (as shown in Figure 7), the hematite lattice structure shows an alteration of iron bilayers and oxygen layers. Ab initio electronic structure calculation, combined with electron transfer theory, reported by Iordanova et al.,[31] shows that the anisotropy of hematite is caused by the slowness of both electron and hole mobilities across basal oxygen planes relative to that within iron bilayers between basal oxygen planes.

However, the 10% Ta-doped sample, which has apparently the strongest (110) orientation (as shown in Figures 6a and 8)

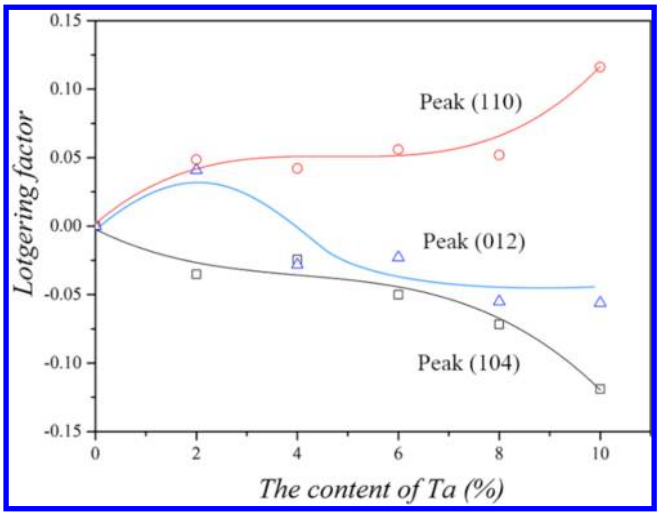


**Figure 8.** Lotgering factor of peak (012) (blue), (104) (black), and (110) (red) for pure and Ta-doped hematite as a function of the content of tantalum.

does not show the highest photoactivity. Note that the peaks (012) and (104) are obviously inhibited in the heavily doped samples, which means that the growth of the high index facets is repressed. Not only the conductivity but also the reactivity of the basal planes has a great influence on the photocatalytic activity of hematite. The reactivity of the metal oxide surfaces is largely determined by the coordinately unsaturated ions, which provide active sites for water oxidation. The density of coordinately unsaturated iron cations of the {001} facet is much lower than that of the high index planes. In recent research,[32] the synthesized hematite nanoplates, enclosed mostly by {001} facets, showed much lower photodegradation ability than the synthesized nanotubes and nanorods, the dominant facets which are {012} and {110}+{001} facets, respectively. In our research, the growth of the high index facets with high photoreactivity are inhibited as the increasing Ta doping content; therefore, the heavily doped hematite shows a much lower photoactivity than the lightly doped ones. Another cause for consideration is that too high concentration of the dopant may lead to segregation of the dopant phase, which will serve as recombination centers and thus inhibit the photoactivity.

To study the influence of the sample fabrication temperature on the phase state of Ta-doped $\alpha$-$Fe_2O_3$, we have obtained the X-ray diffraction spectra for 2% Ta-doped $\alpha$-$Fe_2O_3$ prepared at different temperatures (400, 500, 600, 680 °C) (as shown in Figure 6b). The samples prepared at 400 and 500 °C both only show a $\alpha$-$Fe_2O_3$ phase, and there was a new phase (temporarily identified as $TaO_2F$ (JCPDS 33-0644)) formed as the calcination temperature was higher than ~500 °C in the sample fabrication. The samples for XRD characterization were prepared on a common glass slide, and it is well known that fluorite (the main component is $CaF_2$) is usually added as a flux


dx.doi.org/10.1021/jp500395a | J. Phys. Chem. C XXXX, XXX, XXX−XXX

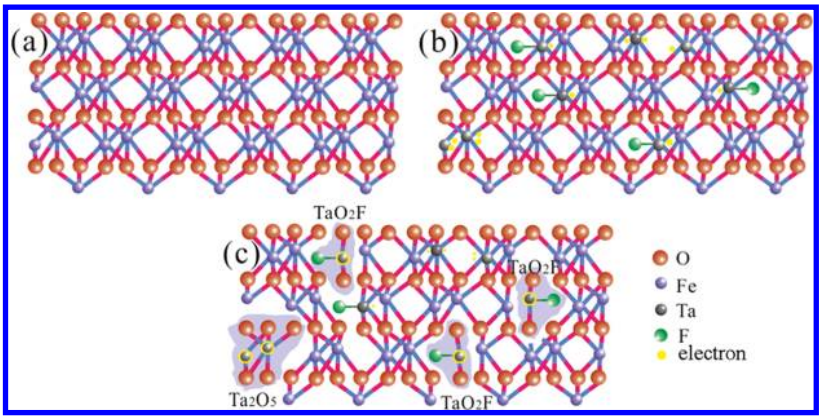


**Figure 9.** Models of hematite crystal lattices: (a) Sample without dopant. (b) Sample doped with Ta and prepared at 500 °C. (c) Sample doped with Ta and prepared at temperature higher than 500 °C.

agent to enhance the fusion of the raw materials in the production of common glass. The samples for PEC performance tests were prepared on FTO glass that contains a certain amount of fluorine. Thus, it is probable for the samples to have some fluorine contamination. When calcined during the sample fabrication, the fluorine in the substrate might diffuse and be incorporated into the hematite thin film. The precursor for the Ta dopant in our research is $TaCl_5$, so there is also the possibility of forming tantalum chloride oxide at higher calcining temperatures. Thus, there are no related standard patterns available for the possible tantalum chloride oxide in addition to the hematite; only $TaO_2F$ is identified in the XRD spectra for samples prepared at higher temperatures. The incorporation of dopants in metal oxide can be described with Kröger–Vink notation.[33] When calcined at high temperature, the precursor $Fe(NO_3)_3$ is decomposed into $\alpha$-$Fe_2O_3$. $Fe^{3+}$ and $O^{2-}$ in the pure hematite crystal are expressed as $Fe_{Fe}^{x}$ and $O_O^x$, respectively, as shown in eq 4

$$Fe(NO_3)_3 \rightarrow Fe_{Fe}^{x} + \frac{3}{2}O_O^x + 3NO_2(g) + \frac{3}{4}O_2(g) \quad (4)$$

In the case of doping hematite with Ta, $Ta^{5+}$ substitutes the $Fe^{3+}$ of the hematite. Because of the different valences between the $Ta^{5+}$ and the substituted $Fe^{3+}$, two extra positive charges produced at each substituted site, which is expressed by the two dots in the superscript of $Fe_{Ta}^{\cdot\cdot}$. Supposing that the mole ratio of Ta:Fe in the Ta-doped hematite is $x/(1-x)$, the doping process is described in the following equation

$$\begin{aligned}(1-x)Fe(NO_3)_3 + xTaCl_5 \\ \rightarrow (1-x)Fe_{Fe}^{x} + xFe_{Ta}^{\cdot\cdot} + \frac{3}{2}O_o^x + xe' \\ + \frac{3}{4}(1-2x)O_2(g) + 3(1-x)NO_2(g) + \frac{5}{2}xCl_2(g)\end{aligned} \quad (5)$$

As expressed in eq 5, to observe the conversion of charge, $2x$ electrons are added. This means that the doping with Ta can increase the electron density in the hematite, which will further improve the conductivity of the material. As previously discussed, the fluorine contained in the glass or in the FTO might diffuse into the hematite lattice and be bonded to the substituent Ta (as described in eq 6). The mechanism previously discussed is also shown in Figure 9a,b.

$$Fe_{Fe}^{\bullet\bullet} + F^- \xrightarrow{Fe_2O_3} Fe^{\bullet} - F \quad (6)$$

While at higher temperatures (e.g., 600, 680 °C), part of the substituted Ta might segregate from the hematite lattice and form $TaO_2F$, as described in eq 7 and in Figure 9c.

$$9Ta^{\bullet} - F + 2O_O^x + e' \xrightarrow{Fe_2O_3} TaO_2F \quad (7)$$

**3.4. Current–Voltage (*I*–*V*) Plot.** To determine whether tantalum dopant altered the dark conductivity of $\alpha$-$Fe_2O_3$, we measured $I$–$V$ characteristics of $\alpha$-$Fe_2O_3$, and 2% Ta-doped $\alpha$-$Fe_2O_3$ prepared at 500 °C was measured in the dark by clamping the two same pieces of samples together (as shown in the scheme of Figure 10), although a more carefully designed

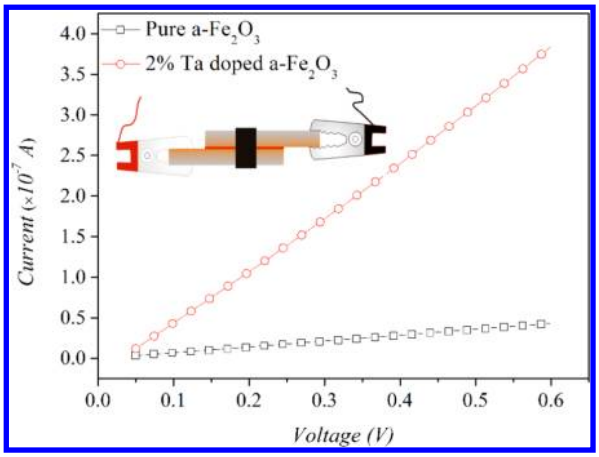


**Figure 10.** $I$–$V$ plots for pure $\alpha$-$Fe_2O_3$ and 2% Ta-doped $\alpha$-$Fe_2O_3$ in the dark. The area of the two samples is 10 mm × 15 mm.

four-point probe configuration needs to be used to measure, more reliably, the conductivity of thin films. The slope of the I–$V$ plots (as shown in Figure 10) were used to estimate the relative conductivity of the samples. The result suggests that the conductivity of $\alpha$-$Fe_2O_3$ is improved up to at least about one order of magnitude by doping with tantalum, which agrees with the electroconductivity measurement reported by Aroutiounian et al.[21]

**3.5. Mott–Schottky Plot.** The Mott–Schottky (M–S) plots for the pure and tantalum-doped $\alpha$-$Fe_2O_3$ photoelectrodes are shown in Figure 11. The flat band potential can be estimated from the Mott–Schottky equation

$$\frac{1}{C_{sc}^2} = \frac{2}{\varepsilon\varepsilon_0 N_D}(E - E_{fb} - kT/e) \quad (8)$$


dx.doi.org/10.1021/jp500395a | J. Phys. Chem. C XXXX, XXX, XXX–XXX

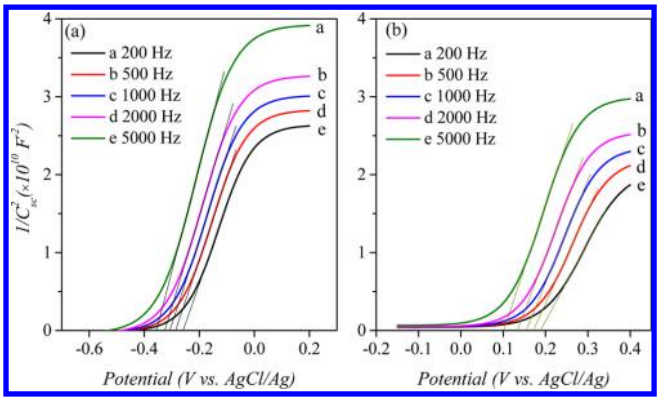


**Figure 11.** Mott–Schottky plots of (a) pure $\alpha$-$Fe_2O_3$ and (b) 2% Ta-doped $\alpha$-$Fe_2O_3$ in 0.1 M $Na_2SO_4$ in the dark.

where $C_{sc}$ is the space-charge capacitance in $F\ cm^{-2}$; e is the electronic charge in $C$; $\varepsilon$ is the dielectric constant of the semiconductor; $\varepsilon_0$ is the permittivity of free space; $N_D$ is the carrier density in $cm^{-3}$; $E$ is the applied potential in V; $E_{fb}$ is the flat band potential in V; $k$ is the Boltzmann constant; and $T$ represents the temperature in $k$. The $(kT/e)$ term can be neglected at room temperature. The flat band potential is obtained from the intercept of the tangent line of the M–S plot on potential axis.

The flat band potential of $\alpha$-$Fe_2O_3$ in 0.1 M $Na_2SO_4$ solution is between −0.27 and −0.36 V (vs Ag/AgCl) at the investigated frequencies. The flat band potential of $\alpha$-$Fe_2O_3$ shifts toward positive direction, from approximately −0.31 to 0.15 V, before and after doping. The flat band potential obtained from Mott–Schottky plots shows a frequency dependency, as shown in Figure 11a,b. This misconvergence might be originated from the nonideality of the photoelectrode surface, which was prepared by a facile and relatively crude method. Thus, a quantitative analysis on the carrier density could not be performed reliably.

**3.6. X-ray Photoelectron Spectroscopy.** XPS survey spectra of pure and Ta-doped $\alpha$-$Fe_2O_3$ films, prepared at 500 °C and have undergone PEC performance test in electrolyte, are shown in Figure 12a. The presence of Ta in doped $\alpha$-$Fe_2O_3$ is confirmed. All samples show strong C peaks, which can be attributed to sample preparation with ethylene glycol as solvent and the contamination of carbon in air. The pure $\alpha$-$Fe_2O_3$ film shows small Sn peaks, which most likely originate from the FTO on the glass substrate. The presence of N in all samples can be attributed to the use of $Fe(NO_3)_3$ as the precursor of $\alpha$-$Fe_2O_3$.

As shown in the XPS of Fe 2p region of the samples (Figure 12b), the spectra are quite similar. The satellite peak (~719.5 eV) of the Fe $2p_{3/2}$ main line can be ascribed to $Fe^{3+}$, and the $Fe^{2+}$ shakeup peak at ~717.2 eV cannot be observed. In the XPS of the O 1s region of all the samples (Figure 12c), there is a shoulder at higher binding energy, which can be attributed to $OH^-$,[34] absorbed on the sample surface during the PEC performance test in electrolyte.

Ta 4f XPS spectra of Ta-doped hematite and $Ta_2O_5$ are shown in Figure 12d. All samples exhibit two peaks, corresponding to Ta $4f_{7/2}$ and Ta $4f_{5/2}$, with a similar area ratio of 4:3 and the same doublet separation energy of 1.8 eV. The two peaks of $Ta_2O_5$ sample are at 27.7 and 25.9 eV, while the relative peaks of Ta-doped hematite samples, at 27.3 and 25.5 eV, shift toward lower binding energy. The binding energy of Ta $4f_{7/2}$ (25.5 eV) is between the values for $Ta_2O_5$ (25.9 eV) and metallic Ta (21.9 eV),[35] suggesting that the $Ta^{5+}$ is incorporated at the $Fe^{3+}$ site in the hematite lattice.

**3.7. UV–Visible Absorption Spectra.** To understand the improved photocatalytic activity, the possible influence of introducing Ta in hematite on electronic band structures was

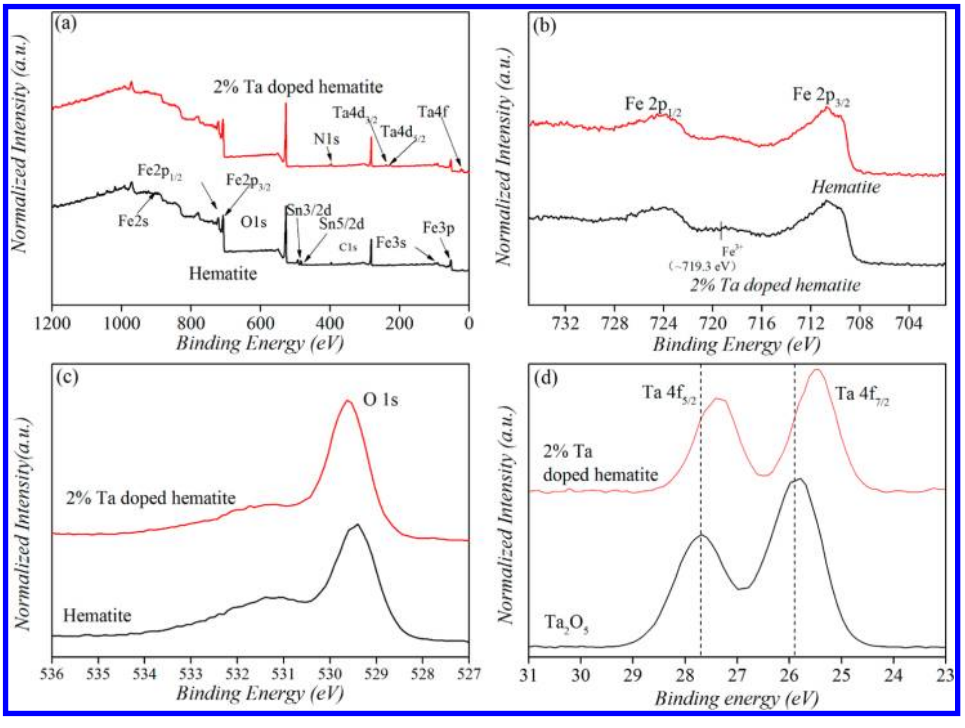


**Figure 12.** XPS survey of (a) pure $\alpha$-$Fe_2O_3$ and 2% Ta-doped $\alpha$-$Fe_2O_3$. High-resolution spectra of (b) Fe 2p, (c) O 1s, and (d) Ta 4f. (The spectra of prepared pure $Ta_2O_5$ were added for comparison.)


dx.doi.org/10.1021/jp500395a | J. Phys. Chem. C XXXX, XXX, XXX–XXX

investigated by UV−visible light absorption spectroscopy. As shown in Figure 13, hematite and Ta-doped hematite have

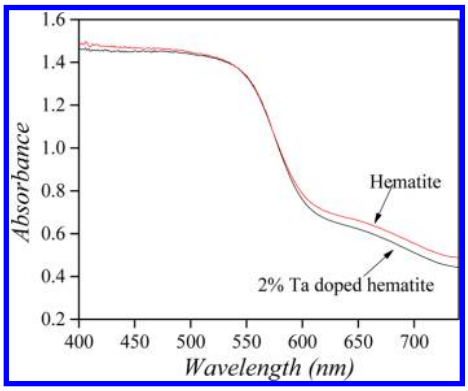


**Figure 13.** UV−visible absorption spectra of pure $\alpha$-$Fe_2O_3$ (red) and 2% Ta-doped $\alpha$-$Fe_2O_3$ (black).

nearly overlapped intrinsic absorption edge with the threshold wavelength of 590 nm, suggesting the unchanged bandgap of hematite by doping Ta in hematite.

**3.8. IPCE Test.** Incident-photon-to-current-efficiencies (IPCE) for pure and Ta-doped hematite were measured at 0.3 and 0.6 V versus Ag/AgCl as a function of incident light wavelength (Figure 14). IPCE can be calculated based on eq 9

$$\mathrm{IPCE}(\%) = \frac{1240 j_{\mathrm{photo}}(\mathrm{mA/cm^2})}{P_{\mathrm{light}}(\mathrm{mW/cm^2}) \times \lambda(\mathrm{nm})} \times 100\% \quad (9)$$

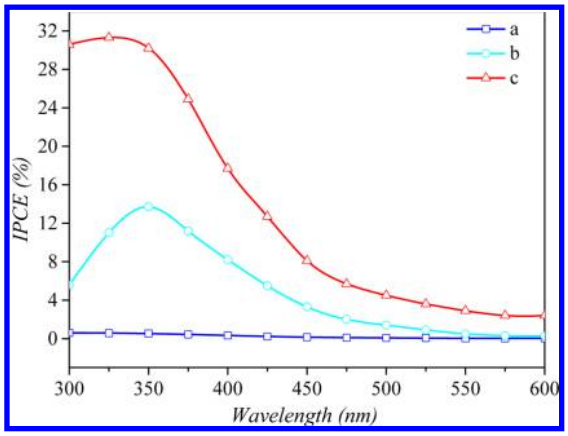


**Figure 14.** Incident photon to current efficiency (IPCE) spectra: (a) pure $\alpha$-$Fe_2O_3$, (b) 2% Ta-doped $\alpha$-$Fe_2O_3$ at 0.3 V versus Ag/AgCl, and (c) 2% Ta-doped $\alpha$-$Fe_2O_3$ at 0.6 V versus Ag/AgCl.

where $j_{\mathrm{photo}}$ is the measured photocurrent density and $P_{\mathrm{light}}$ is the incident light power density for each wavelength, $\lambda$. As shown in Figure 14, the Ta-doped hematite shows a large improvement over the undoped sample in both UV (<420 nm) and visible light (420~600 nm), and a photocurrent onset at 590~600 nm can be observed, which is in accordance with the onset strong light absorption in our UV−visible light absorption spectra (Figure 14). The efficiency rises with the decrease in light wavelength and reaches its maximum at 350 nm, with a value of 14% at 0.3 V versus Ag/AgCl and 32% at 0.6 V versus Ag/AgCl. The maximum has been attributed to the direct transition ($O^{2-}2p^6 \rightarrow Fe^{3+}3d$, $\lambda$ < 400 nm) and not the indirect transition of ($Fe^{3+}3d \rightarrow 3d$, $\lambda$ < 400 nm).[36]

## 4. CONCLUSIONS

Ta has been screened using the SECM method and found to be a highly effective dopant for hematite. The optimized Ta-doped hematite shows a much higher photoactivity than pure hematite even under visible-light irradiation ($\lambda$ > 420 nm). The Ta dopant might serve to improve the conductivity of hematite without enhancing the recombination rate of photocharge carriers and thus enhance the photoactivity. The method we used to fabricate and dope a $\alpha$-$Fe_2O_3$ photoanode is a facile and relatively simple method. Larger enhancement of the PEC performance by the improvement of the synthesis and incorporation of a surface electrocatalyst is expected to improve the water oxidation reaction.

## AUTHOR INFORMATION

### Corresponding Author

*E-mail: ajbard@mail.utexas.edu.

### Present Address

[§]State-Key Laboratory of Chemical Engineering, East China University of Science and Technology, Shanghai 200237, China.

### Author Contributions

The manuscript was written through contributions of all authors.

### Notes

The authors declare no competing financial interest.

## ACKNOWLEDGMENTS

We thank Drs. Yanqing Cong, Hyun Seo Park, Chongyang Liu, Xiaole (Joy) Chen, Sung Ki Cho, and others in this group for their helpful discussions. We also thank Dr. Vincent Lynch, Department of Chemistry and Dr. Hugo Steinfink, Department of Chemical Engineering for their valuable advice about XRD characterization. X.Z. was financially supported by the National Scholarship Fund of the China Scholarship Council (No. 2009674514). This work was funded by the Division of Chemical Sciences, Geosciences, and Biosciences, Office of Basic Energy Sciences of the U.S. Department of Energy through Grant DE-FG02-09ER16119.

## REFERENCES

(1) Hardee, K. L.; Bard, A. J. Semiconductor Electrodes V. The Application of Chemically Vapor Deposited Iron Oxide Films to Photosensitized Electrolysis. *J. Electrochem. Soc.* **1976**, *123*, 1024−1026.

(2) Cesar, I.; Kay, A.; Gonzalez Martinez, J. A.; Grätzel, M. Translucent Thin Film $Fe_2O_3$ Photoanodes for Efficient Water Splitting by Sunlight: Nanostructure-Directing Effect of Si-Doping. *J. Am. Chem. Soc.* **2006**, *128*, 4582−4583.

(3) Kay, A.; Cesar, I.; Grätzel, M. New Benchmark for Water Photooxidation by Nanostructured $\alpha$-$Fe_2O_3$ Films. *J. Am. Chem. Soc.* **2006**, *128*, 15714−15721.

(4) Glasscock, J. A.; Barnes, P. R. F.; Plumb, I. C.; Savvides, N. Enhancement of Photoelectrochemical Hydrogen Production from Hematite Thin Films by the Introduction of Ti and Si. *J. Phys. Chem. C* **2007**, *111*, 16477−16488.

(5) Jorand Sartoretti, C.; Alexander, B. D.; Solarska, R.; Rutkowska, I. A.; Augustynski, J.; Cerny, R. Photoelectrochemical Oxidation of Water at Transparent Ferric Oxide Film Electrodes. *J. Phys. Chem. B* **2005**, *109*, 13685−13692.

(6) Hahn, N. T.; Mullins, C. B. Photoelectrochemical Performance of Nanostructured Ti- and Sn-Doped $\alpha$-$Fe_2O_3$ Photoanodes. *Chem. Mater.* **2010**, *22*, 6474−6482.

(7) Wang, G.; Ling, Y.; Wheeler, D. A.; George, K. E. N.; Horsley, K.; Heske, C.; Zhang, J. Z.; Li, Y. Facile Synthesis of Highly Photoactive $\alpha$-$Fe_2O_3$-Based Films for Water Oxidation. *Nano Lett.* **2011**, *11*, 3503−3509.
(8) Kleiman-Shwarsctein, A.; Huda, M. N.; Walsh, A.; Yan, Y.; Stucky, G. D.; Hu, Y.-S.; Al-Jassim, M. M.; McFarland, E. W. Electrodeposited Aluminum-Doped $\alpha$-$Fe_2O_3$ Photoelectrodes: Experiment and Theory. *Chem. Mater.* **2009**, *22*, 510−517.
(9) Sanchez, C.; Sieber, K. D.; Somorjai, G. A. The Photoelectrochemistry of Niobium Doped $\alpha$-$Fe_2O_3$. *J. Electroanal. Chem. Interfacial Electrochem.* **1988**, *252*, 269−290.
(10) Ling, Y.; Wang, G.; Wheeler, D. A.; Zhang, J. Z.; Li, Y. Sn-Doped Hematite Nanostructures for Photoelectrochemical Water Splitting. *Nano Lett.* **2011**, *11*, 2119−2125.
(11) Bohn, C. D.; Agrawal, A. K.; Walter, E. C.; Vaudin, M. D.; Herzing, A. A.; Haney, P. M.; Talin, A. A.; Szalai, V. A. Effect of Tin Doping on $\alpha$-$Fe_2O_3$ Photoanodes for Water Splitting. *J. Phys. Chem. C* **2012**, *116*, 15290−15296.
(12) Kleiman-Shwarsctein, A.; Hu, Y. S.; Forman, A. J.; Stucky, G. D.; McFarland, E. W. Electrodeposition of $\alpha$-$Fe_2O_3$ Doped with Mo or Cr as Photoanodes for Photocatalytic Water Splitting. *J. Phys. Chem. C* **2008**, *112*, 15900−15907.
(13) Liu, Y.; Yu, Y. X.; Zhang, W. D. Photoelectrochemical Properties of Ni-Doped $Fe_2O_3$ Thin Films Prepared by Electrodeposition. *Electrochim. Acta* **2012**, *59*, 121−127.
(14) Ingler, W. B., Jr.; Khan, S. U. M. Photoresponse of Spray Pyrolytically Synthesized Magnesium-Doped Iron (III) Oxide (p-$Fe_2O_3$) Thin Films Under Solar Simulated Light Illumination. *Thin Solid Films* **2004**, *461*, 301−308.
(15) Gaudon, M.; Pailhé, N.; Majimel, J.; Wattiaux, A.; Abel, J.; Demourgues, A. Influence of $Sn^{4+}$ and $Sn^{4+}/Mg^{2+}$ Doping on Structural Features and Visible Absorption Properties of $\alpha$-$Fe_2O_3$ Hematite. *J. Solid State Chem.* **2010**, *183*, 2101−2109.
(16) Satsangi, V. R.; Kumari, S.; Singh, A. P.; Shrivastav, R.; Dass, S. Nanostructured Hematite for Photoelectrochemical Generation of Hydrogen. *Int. J. Hydrogen Energy* **2008**, *33*, 312−318.
(17) Lee, J.; Ye, H.; Pan, S.; Bard, A. Screening of Photocatalysts by Scanning Electrochemical Microscopy. *Anal. Chem.* **2008**, *80*, 7445−7450.
(18) Ye, H.; Park, H. S.; Bard, A. J. Screening of Electrocatalysts for Photoelectrochemical Water Oxidation on W-Doped $BiVO_4$ Photocatalysts by Scanning Electrochemical Microscopy. *J. Phys. Chem. C* **2011**, *115*, 12464−12470.
(19) Jang, J. S.; Lee, J.; Ye, H.; Fan, F. R. F.; Bard, A. J. Rapid Screening of Effective Dopants for $Fe_2O_3$ Photocatalysts with Scanning Electrochemical Microscopy and Investigation of Their Photoelectrochemical Properties. *J. Phys. Chem. C* **2009**, *113*, 6719−6724.
(20) Jang, J. S.; Yoon, K. Y.; Xiao, X.; Fan, F. R. F.; Bard, A. J. Development of a Potential $Fe_2O_3$-Based Photocatalyst Thin Film for Water Oxidation by Scanning Electrochemical Microscopy: Effects of Ag-$Fe_2O_3$ Nanocomposite and Sn Doping. *Chem. Mater.* **2009**, *21*, 4803−4810.
(21) Aroutiounian, V. M.; Arakelyan, V. M.; Shahnazaryan, G. E.; Stepanyan, G. M.; Turner, J. A.; Khaselev, O. Investigation of Ceramic $Fe_2O_3$ <Ta> Photoelectrodes for Solar Energy Photoelectrochemical Converters. *Int. J. Hydrogen Energy* **2002**, *27*, 33−38.
(22) Anpo, M.; Takeuchi, M. The Design and Development of Highly Reactive Titanium Oxide Photocatalysts Operating Under Visible Light Irradiation. *J. Catal.* **2003**, *216*, 505−516.
(23) Shannon, R. Revised Effective Ionic Radii and Systematic Studies of Interatomic Distances in Halides and Chalcogenides. *Acta Crystallogr., Sect. A* **1976**, *32*, 751−767.
(24) Lotgering, F. K. Topotactical Reactions with Ferrimagnetic Oxides Having Hexagonal Crystal Structures-I. *J. Inorg. Nucl. Chem.* **1959**, *9*, 113−123.
(25) Lučić Lavčević, M.; Bernstorff, S.; Dubček, P.; Jozić, D.; Jerković, I.; Marijanović, Z. GISAXS/GIXRD View of ZnO Films with Hierarchical Structural Elements. *J. Nanotechnol.* **2012**, *2012*, 10.
(26) Chiu, H. M.; Chang, Y. T.; Wu, W. W.; Wu, J. M. Synthesis and Characterization of One-Dimensional Ag-doped ZnO/Ga-doped ZnO Coaxial Nanostructure Diodes. *ACS Appl. Mat. Interfaces* **2014**, DOI: 10.1021/am500470y.
(27) Merschjann, C.; Mews, M.; Mete, T.; Karkatzinou, A.; Rusu, M.; Korzun, B. V.; Schorr, S.; Schubert-Bischoff, P.; Seeger, S.; Th, S.-N.; et al. $AgGaSe_2$ Thin Films Grown by Chemical Close-Spaced Vapor Transport for Photovoltaic Applications: Structural, Compositional and Optical Properties. *J. Phys.: Condens. Matter* **2012**, *24*, 175801.
(28) *Lange's Handbook of Chemistry*, 15th ed.; Dean, J. A., Ed.; McGraw Hill Book Co.: New York, 1999; pp 41−53.
(29) Reeves, N. J.; Mann, S. Influence of Inorganic and Organic Additives on the Tailored Synthesis of Iron Oxides. *J. Chem. Soc., Faraday Trans.* **1991**, *87*, 3875−3880.
(30) Yang, H. G.; Sun, C. H.; Qiao, S. Z.; Zou, J.; Liu, G.; Smith, S. C.; Cheng, H. M.; Lu, G. Q. Anatase $TiO_2$ Single Crystals with a Large Percentage of Reactive Facets. *Nature* **2008**, *453*, 638−641.
(31) Iordanova, N.; Dupuis, M.; Rosso, K. M. Charge Transport in Metal Oxides: A Theoretical Study of Hematite $\alpha$-$Fe_2O_3$. *J. Chem. Phys.* **2005**, *122*, 144305.
(32) Zhou, X.; Lan, J.; Liu, G.; Deng, K.; Yang, Y.; Nie, G.; Yu, J.; Zhi, L. Facet-Mediated Photodegradation of Organic Dye Over Hematite Architectures by Visible Light. *Angew. Chem., Int. Ed.* **2012**, *51*, 178−182.
(33) Kröger, F. A. *The Chemistry of Imperfect Crystals*; North-Holland Pub. Co.: Amsterdam, 1964.
(34) McIntyre, N. S.; Zetaruk, D. G. X-ray Photoelectron Spectroscopic Studies of Iron Oxides. *Anal. Chem.* **1977**, *49*, 1521−1529.
(35) McGuire, G. E.; Schweitzer, G. K.; Carlson, T. A. Core Electron Binding Energies in Some Group IIIA, VB, and VIB Compounds. *Inorg. Chem.* **1973**, *12*, 2450−2453.
(36) Kennedy, J. H.; Frese, K. W. Photooxidation of Water at $\alpha$-$Fe_2O_3$ Electrodes. *J. Electrochem. Soc.* **1978**, *125*, 709−714.